

Zooming Out on Zooming In: Advancing Super-Resolution for Remote Sensing

Piper Wolters Favyen Bastani Aniruddha Kembhavi
 Allen Institute for AI
 {piperw, favyenb, anik}@allenai.org

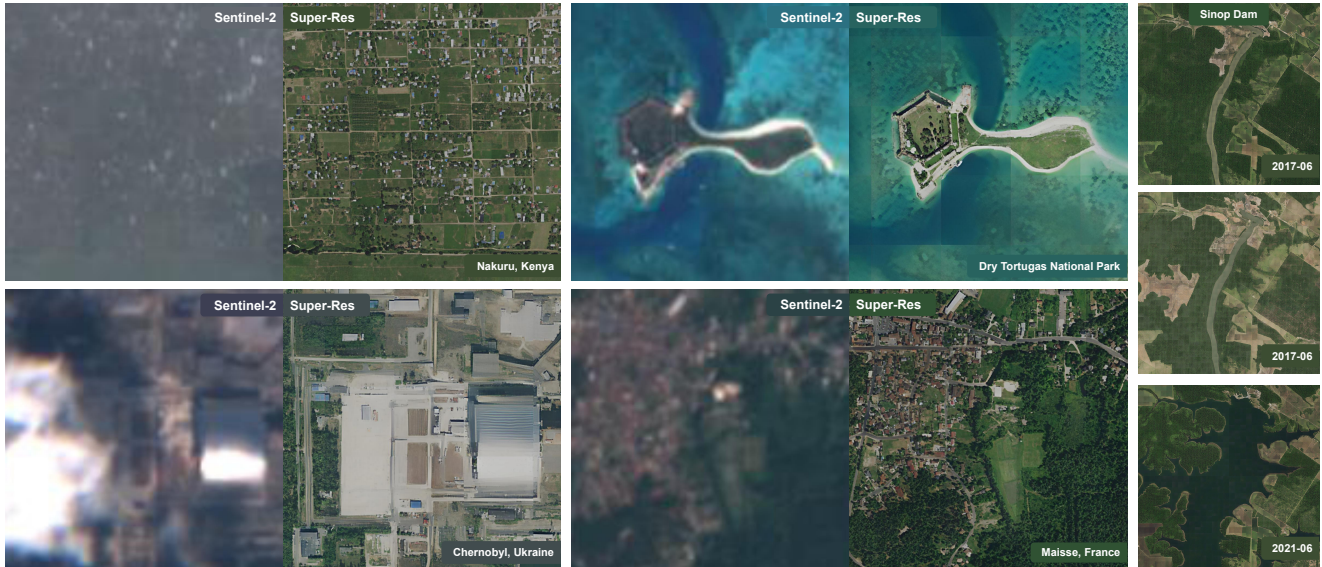


Figure 1. Display of the incredible power of super-resolution for remote sensing imagery. High-resolution satellite imagery is not available for free worldwide, and a public source such as NAIP is restricted to every 2-3 years in the US. On the other hand, Sentinel-2 imagery is global, free, and has a revisit rate of 5-10 days, so with super-resolution methods, we can generate high-resolution imagery globally and frequently, especially in places that have disproportionately less public imagery.

Abstract

Super-Resolution for remote sensing has the potential for huge impact on planet monitoring by producing accurate and realistic high resolution imagery on a frequent basis and a global scale. Despite a lot of attention, several inconsistencies and challenges have prevented it from being deployed in practice. These include the lack of effective metrics, fragmented and relatively small-scale datasets for training, insufficient comparisons across a suite of methods, and unclear evidence for the use of super-resolution outputs for machine consumption. This work presents a new metric for super-resolution, CLIPSCORE, that corresponds far better with human judgments than previous metrics on an extensive study. We use CLIPSCORE to evaluate four standard methods on a new large-scale dataset, S2-NAIP, and three existing benchmark datasets, and find that generative adversarial networks easily outperform more traditional L2 loss-based models and are more semantically

accurate than modern diffusion models. We also find that using CLIPSCORE as an auxiliary loss can speed up the training of GANs by 18x and lead to improved outputs, resulting in an effective model in diverse geographies across the world which we will release publicly. The dataset, pre-trained model weights, and code are available at [this URL](#).

1. Introduction

High-resolution satellite and aerial imagery have the potential to change the landscape of environmental and climate monitoring applications. Images from these sensors provide the ability to count individual trees [65], classify crop types and conditions [35], map out detailed land use categories [31] and track glacial conditions [55]. Low resolution imagery limits these observations to coarse designations of regions such as forest, farmland, residential or ice. Public high-resolution imagery is available infrequently in a few developed countries and commercial global imagery

is expensive and can be five or more years out of date. With the bounded spatio-temporal coverage of public domain high-resolution imagery and cost-prohibitive commercial imagery, many use cases cannot be scaled up globally.

This lack of free high-resolution imagery has prompted research in **Super-Resolution for Remote Sensing**, where computer vision methods are used to upsample low-resolution imagery. Past works include spline models [3], convolutional neural networks [11, 26] and generative networks [32, 54]. Within this field are diverse datasets with varying satellites, spatial resolutions [25, 42] and earth coverage [40, 42]. Despite this attention and potential for impact, Super-Resolution (SUPER-RES) for remote sensing faces many challenges that are limiting progress.

First, metrics for SUPER-RES have serious and well known issues, see Figure 2. It is crucial to establish a metric that closely aligns with human perception and reflects the accuracy and realism of SUPER-RES outputs. We run an extensive human evaluation study to assess the quality of SUPER-RES outputs, and then compare human preferences to those of multiple pixel-wise, perceptual, and model-based metrics. We determine that model-based metrics easily outperform pixel-wise ones, and that using modern and powerful visual encoders is most effective. Based on this analysis and inspired by [20], we propose a new metric for this domain, CLIPSCORE.

Second, existing remote sensing datasets are relatively small in comparison to those for natural images (see Table 1), and often imagery is sourced from commercial vendors, making it expensive to deploy models in practice. We present a new large-scale public domain remote sensing SUPER-RES dataset, covering 113K km^2 using free imagery from Sentinel-2 [1] and the US National Agriculture Imagery Program (NAIP). There are at least 18 Sentinel-2 images for each NAIP image (to support multi-view super-resolution), along with geographic and temporal metadata. This large amount of free imagery allows us to determine that scaling up indeed increases performance, and models can be continually updated with the reoccurring public data for years to come.

Third, while many diverse models have been proposed, rarely are models compared side-by-side, especially models that are biased towards the simple and shallow metrics PSNR and SSIM [11, 34, 43, 50] with models that are more geared towards perceptual quality [2, 32, 56, 57]. We perform comprehensive experiments on four remote sensing SUPER-RES datasets with two L2 loss-based methods, a GAN, and a diffusion model. We find that the L2 loss-based methods lag behind by large margins and that the GAN outperforms other methods in terms of our newly proposed metric, CLIPSCORE (and also the popular LPIPS metric) on all four datasets. We also find that training GANs with a CLIPScore based loss speeds up training dramatically (18x speedup) and further improves performance. With the in-

creasing emphasis on avoiding hallucinations by generative methods, we run a human study to determine the accuracy of human made structures and find that the GAN is superior to the diffusion model. This body of evidence suggests that despite GANs falling out of favor to modern diffusion models, particularly in the natural image domain, they nevertheless perform really well and provide much faster inference for remote sensing SUPER-RES.

Fourth, while there is some work exploring the use of SUPER-RES images as input to downstream tasks [14] in lieu of the original low-resolution images, the evidence of improvement over directly inputting the low-resolution images is unclear. And although representation learning has received much interest in computer vision, the use of SUPER-RES as a representation learning mechanism is under-explored. We conduct a set of experiments to address both of these directions and find that SUPER-RES is a powerful representation learning mechanism that shows promise on downstream remote sensing tasks; but also find that training models on SUPER-RES outputs may not yet be more effective than training on the original low-resolution images for these tasks. Based on these findings, we establish that although SUPER-RES outputs can have a large impact for planet monitoring, they are primarily effective for human consumption (visualization); more progress is required for them to be effective for machine consumption.

We leverage our findings to build an effective model for SUPER-RES that works well in diverse geographies. Furthermore, we deploy the model globally to regularly compute up-to-date high-resolution imagery that is freely available. All data, code, models, and pretrained weights are available at [this URL](#).

In summary, our contributions are:

1. CLIPSCORE, a new metric for SUPER-RES that strongly corresponds with human preferences.
2. S2-NAIP, a large-scale, public-domain dataset for remote-sensing SUPER-RES.
3. An extensive evaluation of SUPER-RES methods on four remote sensing datasets, and a determination that GANs are the current state-of-the-art.
4. Demonstrating that transferring SUPER-RES weights to downstream tasks works well, but machine consumption of SUPER-RES outputs is ineffective.
5. A new global model for SUPER-RES that leverages the above contributions.

2. Related Work

SUPER-RES has a rich history in computer vision [12, 30, 59, 69], with recent methods achieving very impressive results [24, 66]. This paper will focus on SUPER-RES for remote sensing, hence we provide context for this domain.

Remote Sensing Super-Resolution Metrics. The two most widely used metrics in SUPER-RES are Peak Signal to Noise Ratio (PSNR) and Structural Similarity Index Mea-

sure (SSIM) [61]. PSNR is a pixel-based metric that is the inverse of an L2 loss; and SSIM was proposed as a perceptual metric based on image qualities like luminance and contrast. They are both simple functions, as briefly addressed by [5, 25], that are unable to handle ambiguities like shadow direction or nadir angle and physical changes like crop harvest cycles. Figure 2 shows how these are not influenced by crucial perceptual nuances such as blur. Märtens et al. [42] propose cPSNR, a variation of PSNR that handles misalignment and brightness differences but the lack of contextual information remains an issue.

Drawbacks with standard metrics have prompted perceptual metrics like Learned Perceptual Image Patch Similarity (LPIPS) [68], which is proven to align with human judgement and is adopted in the natural image domain [6, 17, 44]. Still, much of the remote sensing community only reports SSIM or pixel-wise metrics [41, 49, 50], including two of the most recently proposed super-resolution benchmarks, SEN2VEN μ S and WorldStrat [10, 39]. We take inspiration from CLIPScore [20] to find a new metric for SUPER-RES.

Remote Sensing Super-Resolution Datasets. Existing datasets can be categorized based on the satellite sensors used, whether they are targeting single image SUPER-RES [39, 56] or multi-image SUPER-RES [10, 25, 42], and the scale of the data, both in km^2 covered and number of pixels.

Many datasets curate pairs of low-resolution and high-resolution images, from one [42] or multiple [10, 34, 39, 56] sensors. In multi-sensor datasets, many utilize Sentinel-2 as the low-resolution image source [10, 25, 39], likely because it is free and maintains a good balance of spatial resolution and temporal revisits. Other works obtain imagery from sources such as Google Earth [13], PlanetScope [48], PeruSAT [45], China GF 1 [62] and WorldView [25].

Even with the many datasets that are intended to be standard benchmarks for remote sensing SUPER-RES [10, 25, 39, 56], there are still papers that evaluate their methods on piecemeal datasets [45, 46, 57]. Also, synthetic datasets are often generated by bicubically downsampling high-resolution images to create artificial pairs [2, 36, 64], which is unrealistic and biased by standard metrics.

Of the proposed benchmark datasets, none of them are large-scale nor are they entirely obtained from free sources. In this paper, we present S2-NAIP, a large-scale dataset with over 1.2 million pairs of public domain images, covering 113 thousand km^2 . Table 1 shows information about existing benchmarks in comparison to S2-NAIP.

Remote Sensing Super-Resolution Methods. Broadly, recent SUPER-RES methods fall into the categories of convolutional [11, 41, 50], generative adversarial [54, 56, 64], and diffusion models [2, 18, 32]. There is a lack of evaluations across these three diverse method families, likely because it is difficult to compare them without strong and consistent metrics. We provide a comprehensive analysis on methods from each of these categories on four remote sens-

	Sensors	Pairs	Input	HR Res.	km^2
S2-NAIP	S2,NAIP	1,200K	18	512x512	113K
SEN2VEN μ S	S2,VEN μ S	133K	1	256x256	0.806K
WorldStrat	S2,SPOT	4K	16	1054x1054	10K
OLI2MSI	LandSat,S2	5.225K	1	480x480	0.2K
PROBA-V	PROBA-V	2.368K	19	384x384	3,000K
MuS2	S2,WV-2	0.091K	14	1965x1686	2.5K

Table 1. Metadata about existing datasets: the low-resolution (LR) and high-resolution (HR) sensors used, the number of HR, LR pairs, the number of LR input images, the spatial resolution of HR (HR Res.) and coverage in terms of km^2 .

ing SUPER-RES datasets, enabling us to determine the most effective method type for remote sensing SUPER-RES. A tangentially related line of work uses older images of a reference image as input to the model along with the low resolution image at the desired timestamp [19]; this produces impressive results, but requires high resolution imagery at inference time, which limits its use in practice.

3. Metrics

PSNR and SSIM are the most commonly used metrics to evaluate SUPER-RES outputs for remote sensing. These metrics however, have many inherent issues. Previous work in the natural image domain has acknowledged these, including the well-known finding that blurring an image will cause significant perceptual change but little difference will be reflected in PSNR [68]. Figure 2 showcases this in the remote sensing domain. Although the two SUPER-RES outputs on the right are quite poor, with one being blurry and the other being sharply downsampled and disfiguring structures, they attain high PSNR and SSIM scores, far beyond an image output from an ESRGAN model which resembles the ground truth image far more closely to the human eye. We now present an extensive human evaluation study to evaluate a suite of metrics and present an image similarity metric based on CLIP [47].

3.1. Super-Resolution Human Judgement Dataset

To find a metric that can effectively assess perceptual quality of remote sensing SUPER-RES outputs, we run a human evaluation study to gather a dataset of human judgements on our S2-NAIP dataset and WorldStrat [10]. Preferences are gathered using Amazon Mechanical Turk (AMT), where each AMT worker was asked to pick, between two model outputs, which one is closer to the target image.

Pairs of outputs were chosen from a set of generated outputs from multiple models on each of 20,000 datapoints from S2-NAIP and 381 datapoints from the WorldStrat. A total of 11,524 pair-wise annotations were collected. More details on this process are in supplementary Section A.1.

We computed many metrics on the model outputs and generated preferences for each of the pairs that had been annotated. The metrics include PSNR, SSIM, LPIPS, SAM-

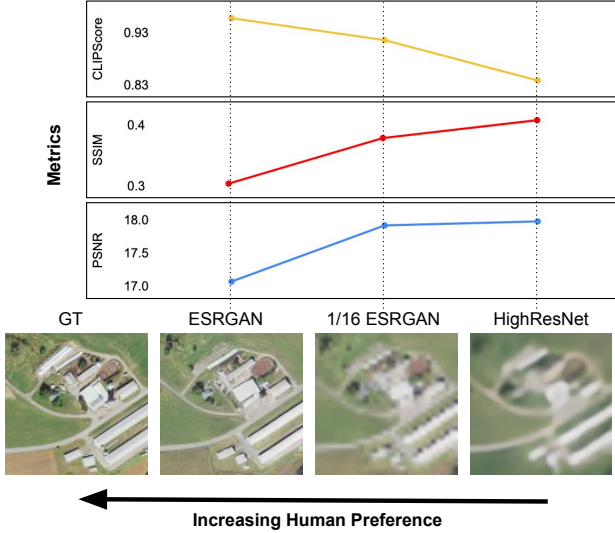


Figure 2. Example of a target image (GT), an ESRGAN output at full resolution as well as downsampled 16x, and a HighResNet output, with corresponding metrics. Note that the four images are ordered from best to worst based on human preference, and PSNR and SSIM increase in an opposite trend. Our proposed CLIPScore more closely matches human judgement.

Score [29], and measures of feature similarity from several web-scale models like CLIP [47]. The level of agreement between each metric and the human preferences across all pairs was computed (i.e., the percentage of pairs where the metric and human pick the same model output as being more similar to the target image). Results are shown in Figure 3.

Finding 1. PSNR and SSIM, the most widely used metrics, are insufficient and poorly correlate with human judgments.

The correspondences between human preferences and those computed by the standard SUPER-RES metrics, PSNR, SSIM, and cPSNR, are very low, as shown in Figure 3. In this study, an accuracy of 50% is equal to random guessing, so metrics with accuracies less than or equal to this are unacceptable for evaluation of SUPER-RES quality. This finding aligns with the counter-intuitive values of these metrics in Figure 2. Remote sensing SUPER-RES should not rely on metrics like PSNR or SSIM when there are other metrics that achieve over 80% accuracy.

3.2. CLIP as an Image Similarity Metric

Inspired by CLIPSCORE [20], we propose a new metric for SUPER-RES that measures the distance in image embedding space between the target image and the generated image, using the web-scale CLIP [47] model. The score is equal to the cosine similarity between the target and output features. This can be done in just a few lines of code, as shown in the snippet below.

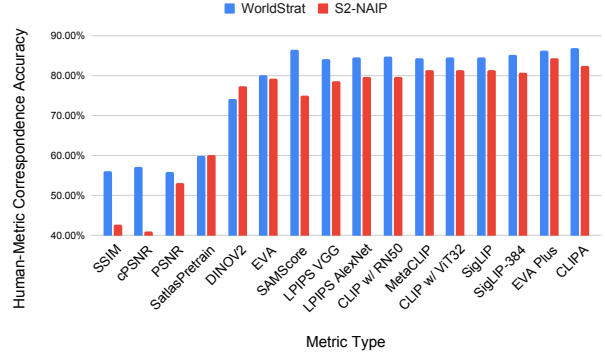


Figure 3. The level of accuracy between human preferences and those generated by the various metrics. The x-axis is ordered from worst to best average accuracy between the two datasets. The y-axis is adjusted to a range of 40% to 90% to better show the difference in accuracy across metrics.

```

1 import clip
2 import torch.nn.functional as F
3
4 # Substitute any CLIP model here
5 clip_model = clip.load("RN50")
6
7 gt_feats = clip_model(gt)
8 super_res_feats = clip_model(super_res)
9
10 score = F.cosine_similarity(gt_feats,
    super_res_features)

```

We assessed several CLIP variants, including CLIPA [27], SigLIP [67], MetaCLIP [63], and EVA [53]. Additionally, we trained variations of CLIP from scratch on satellite imagery, similar to [23], but found the performance of these, as metrics, to be worse than the pretrained models. More details are provided in supplementary Section A.2.

Finding 2. CLIP is an effective super-resolution metric.

The results from the human-metric correspondence study show that the CLIP models are effective at measuring perceptual quality, with at least 76% agreement with human preference. CLIPA-v2 [28] performed best in this study, with an impressive agreement accuracy of 84.6%. We propose this as a measure of image similarity for SUPER-RES.

We use the open-source CLIPA-v2 model with the ViT-bigG-14 architecture, pretrained on DataComp1b [15], from the open_clip codebase [8]. Note that this model configuration is in the top-5 of best performing models on their set of 38 evaluation tasks including the remote sensing tasks Resisc45 [7] and FMoW [9]. The large diversity in the DataComp1b training data is likely a contributing factor to why this model works so well as a metric for satellite imagery.

4. Data

Existing datasets are relatively small in scale, in terms of number of images and coverage in terms of km^2 , as re-

Method	S2-NAIP			WorldStrat			PROBA-V			OLI2MSI		
	cPSNR \uparrow	LPIPS \uparrow	CLIP \uparrow	cPSNR \uparrow	LPIPS \uparrow	CLIP \uparrow	cPSNR \uparrow	LPIPS \uparrow	CLIP \uparrow	cPSNR \uparrow	LPIPS \uparrow	CLIP \uparrow
SRCNN	17.9039	0.3517	0.7	31.5746	0.4493	0.6196	23.9455	0.2112	0.7924	43.4113	0.7614	0.9285
HighResNet	20.9171	0.199	0.6705	32.8787	0.4416	0.5998	22.5687	0.2137	0.8096	35.7374	0.86	0.94
ESRGAN	22.6506	0.8406	0.8745	31.723	0.8299	0.9842	24.9336	0.2154	0.8465	36.3202	0.8709	0.9518
SR3	19.4706	0.6292	0.8223	30.545	0.7745	0.9232	23.7789	0.2115	0.8115	34.2208	0.839	0.9391

Table 2. Results for four methods on four datasets. The reported LPIPS scores are converted to an accuracy, so with each of these metrics, higher is better. ESRGAN achieves the best CLIPSCORE for all datasets, and that is the metric we are prioritizing for this study.

flected in Table 1. Also, most datasets source a portion of their imagery from commercial satellites, making it difficult in practice to extend the data and methods produced.

4.1. S2-NAIP Dataset

We build a new dataset, S2-NAIP, consisting of 1.2 million pairs of low-resolution Sentinel-2 time series and high-resolution NAIP images. The goal with this is to measure if an increased scale of training data will improve model performance as well as to release a remote sensing SUPER-RES dataset **built entirely from public domain images**.

NAIP imagery covers most of the United States with a revisit rate of 2-3 years, and Sentinel-2 is globally available with new imagery every 5-10 days. We source the NAIP imagery from 2019-2020 as well as all spatially overlapping Sentinel-2 images within two months of each NAIP image capture timestamp, resulting in at least 18 Sentinel-2 images. We do not remove images with cloud cover, so that the data maintains a real-world distribution.

The full resolution of each NAIP *tile* is 512x512 pixels. Tiles correspond to Web-Mercator tiles at zoom level 17, i.e., the world is projected to a 2D plane and divided into a $2^{17} \times 2^{17}$ grid, with each tile corresponding to a grid cell. Each NAIP tile corresponds to a time series of Sentinel-2 images, each having a resolution of 32x32 pixels. Geospatial and temporal information for all imagery is provided.

With the goal of avoiding an overload of monotonous landscapes such as ocean or desert, we sample NAIP tiles from within 20km of cities with populations of at least 20k. This resulted in a balance of various man-made infrastructure like water tanks, parking lots, and houses as well as farmland, mountainous area, and forest.

We train an ESRGAN [58], as described in Section 5, to upsample the Sentinel-2 images by a factor of four to 128x128 pixels, and use NAIP tiles downsampled by four as the target images. Experiments are run with 1, 3, 10, 30, and 100 percent of the S2-NAIP dataset to determine the difference in performance with varied dataset sizes.

Additionally, we train three sizes of the ESRGAN model on each of these data splits to see if increased model size in conjunction with more data is correlated with better outputs. We define small, medium, and large versions of the ESRGAN with 17mil, 87mil, and 347mil parameters, respectively. Although the effects of data and model size are well studied in the natural image domain, few comprehensive studies have been done on this in remote sensing.

Finding 3. Performance scales with dataset and model size.

Somewhat unsurprisingly, we find that training on more of S2-NAIP results in higher performance, as shown in Figure 5. Between the smallest and largest data splits, there is a ten point improvement in CLIPSCORE for the smallest model. This suggests that training on larger amounts of data will be beneficial to SUPER-RES in remote sensing, justifying the creation of large-scale datasets like our proposed S2-NAIP.

Model size also contributes to higher quality outputs. There is on average a five point improvement between the small and large models across all five data splits. This finding motivates further exploration into larger SUPER-RES models for satellite imagery, especially with GANs that provide substantially faster inference than diffusion models.

5. Method Study

We run a comprehensive study with SRCNN [12], HighResNet [11], [10], ESRGAN [58], and Image Super-Resolution via Iterative Refinement (SR3); the latter method is an adaption of Denoising Diffusion for Probabilistic Models (DDPM) [22] for SUPER-RES. The SR3 model has 97mil parameters so we choose to use the medium ESRGAN from Figure 5 which has 87mil parameters, for a relatively fair comparison. Minor model tweaks are made across datasets to account for different upsample factors as well as for stabilization of training. Specific training and model details can be found in supplementary Section A.3.

We train and evaluate these methods on our proposed large-scale S2-NAIP dataset as well as the existing PROBA-V [42] and the recently proposed benchmarks WorldStrat [10] and OLI2MSI [56]. We report CLIPSCORE as proposed in Section 3 and base our evaluation on this metric, though we also report cPSNR and LPIPS for the sake of comparison to previous work. Results are shown in Table 2.

We further experimented with several variations of ESRGAN and describe the findings that led to demonstrably better performance in Section 6. We also ran experiments using Denoising Diffusion Implicit Models (DDIM) [51], which led to much faster inference but slightly lesser quality outputs; as well as Classifier Free Guidance [21], which did not clearly improve output quality. Further details with sample outputs can be found in supplementary Section A.4.

Finding 4. GANs are capable super-resolution methods.

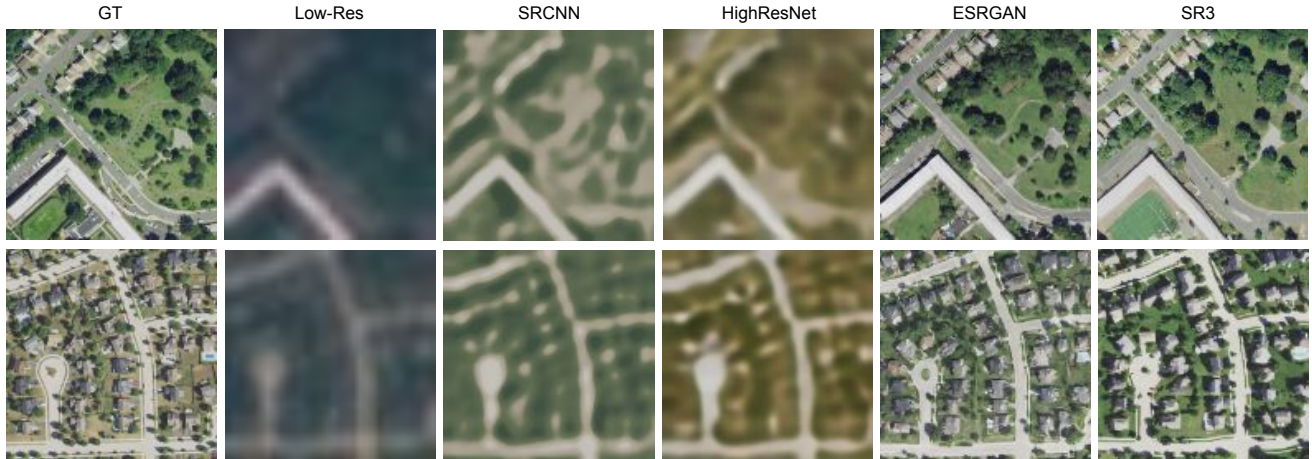


Figure 4. Examples of target images (GT), one of the corresponding low-resolution images (Low-Res), and SUPER-RES outputs from SRCNN, HighResNet, Medium ESRGAN, and SR3 on samples from the S2-NAIP dataset. We recommend zooming in for the full effect.

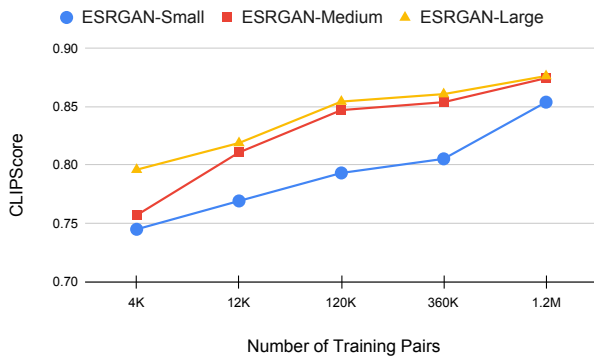


Figure 5. CLIPSCORE results on the S2-NAIP dataset, with three sizes of the ESRGAN model and five data splits. Performance increases with more data and larger models.

Based on the cumulative CLIPSCORE results on four datasets as shown in Table 2, it is clear that ESRGAN is effective in producing high-quality SUPER-RES outputs. Compared to training only on L2 loss, like SRCNN and HighResNet, the outputs are sharper and more similar to the target images, as shown in Figure 4.

Although diffusion models have become increasingly popular in computer vision, GANs are proving here to be very effective. It is also important to mention the large gap in inference speed – GANs require just one forward pass while diffusion models require several. Between our ESRGAN and SR3 models, the ESRGAN is 200x faster.

Building Count Study. Qualitative assessments of the four models, as shown in Figure 4, provides evidence that ESRGAN and SR3 produce high quality outputs. A priority in remote sensing SUPER-RES is maintaining accuracy and avoiding hallucinations [42]. To determine the accuracy of the two generative methods, we run a human study on a held

out set of 256 datapoints from S2-NAIP, with the task of counting buildings. We choose this task because human-made structures are of special interest in satellite imagery and are important to represent accurately.

We have an expert annotator count the number of visible buildings in the provided target images as well as the corresponding generated images from ESRGAN and SR3. Of the buildings annotated in each model output, the buildings were labeled as ground truth or hallucination, depending on if the building exists in the target image or not.

Results from this study show that **ESRGAN accurately generates the buildings from the high-resolution target image 94.70% of the time**, while SR3 only 81.77% of the time. Furthermore, the average hallucination rate for each method is 0.41 and 0.43 buildings per image, respectively.

Finding 5. *Diffusion models generate realistic but inaccurate images.*

Results from this study give us a glimpse into the difference in semantic accuracy between two models that both generate high perceptual quality outputs. ESRGAN is more accurate in generating the correct buildings relative to the target image and has a smaller hallucination rate.

Example qualitative outputs from the building count study are shown in Figure 6, where red circles point out flaws in the SR3 column such as nonexistent roads, the addition of buildings where there should be none, and a grassy field where there is supposed to be a river.

6. Improving ESRGAN

We find ESRGAN to be the strongest SUPER-RES method of the four compared in our study, and propose novel techniques to improve it. This includes adding an auxiliary loss based on CLIPSCORE described in Section 6.1 and incorporating domain knowledge into the training pipeline, de-



Figure 6. Examples of high-resolution images from S2-NAIP and corresponding ESRGAN and SR3 outputs. Red circles showcase qualitatively incorrect portions generated by SR3.

scribed in supplementary Section A.5. We hypothesize that these could be transferred to other GAN models.

6.1. Training with CLIPScore

Similar to previous works that optimize a loss that is inversely related to a metric such as LPIPS [68], we introduce a CLIPSCORE loss. We use an L1 loss to minimize the distance between CLIP features of the target and the SUPER-RES output. In our experiments, we use CLIP with ResNet50, as it is smaller and thus faster than CLIPA-v2.

We train the small ESRGAN in Figure 5, from scratch, with the addition of the CLIPSCORE loss. Figure 7 shows results of models trained with and without this loss.

Finding 6. *Incorporating CLIP significantly speeds up training and produces more effective models.*

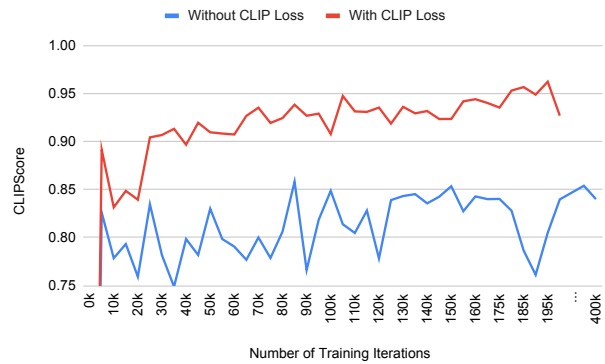


Figure 7. Plot of CLIPScore between a model trained with the CLIP-based loss and one without. Note the y-axis is between 0.75 and 0.95 to more clearly show the difference in performance.

We find that training a model with the addition of the CLIPScore-based loss results in a **9 point improvement in CLIPScore in 18x less training time**. This decreases our training time from weeks to hours and the quality of SUPER-RES outputs is vastly improved.

The Best Model. We compile all of the improvements described in Sections 6.1 and supplementary Section A.5 into one model, and the result is an impressive 0.959 CLIPSCORE. Figure 8 shows qualitative results between the small and large ESRGAN models from Figure 5, compared to the best model.

7. Super-Resolution for Downstream Tasks

In this section, we analyze two uses of SUPER-RES for downstream tasks: images and features.

We compile a set of five downstream tasks corresponding to existing datasets: the three SatlasPretrain fine-tuning datasets (solar farms, wind turbines, and marine infrastructure) [4], PASTIS (crop type segmentation) [16], and BigEarthNet (land cover segmentation) [52]. Because these five datasets are built with Sentinel-2 imagery in mind, most features are relatively coarse, so we also create a new urban land use segmentation dataset from OpenStreetMap labels; details are in supplementary Section A.6.

7.1. Image Usage

Previous works such as PROBA-V and WorldStrat [10, 42] have argued that SUPER-RES outputs could be used in place of low-resolution images for downstream tasks like crop type and urban land use segmentation. In fact, the authors of PROBA-V argue that, in remote sensing, SUPER-RES methods should be designed for machine rather than human consumption, and suggest that models trained without GAN losses may produce images with more accurate pixel values that are better for machine consumption.

To evaluate this claim, we generate SRCNN, HighResNet, and ESRGAN SUPER-RES outputs from the Sentinel-

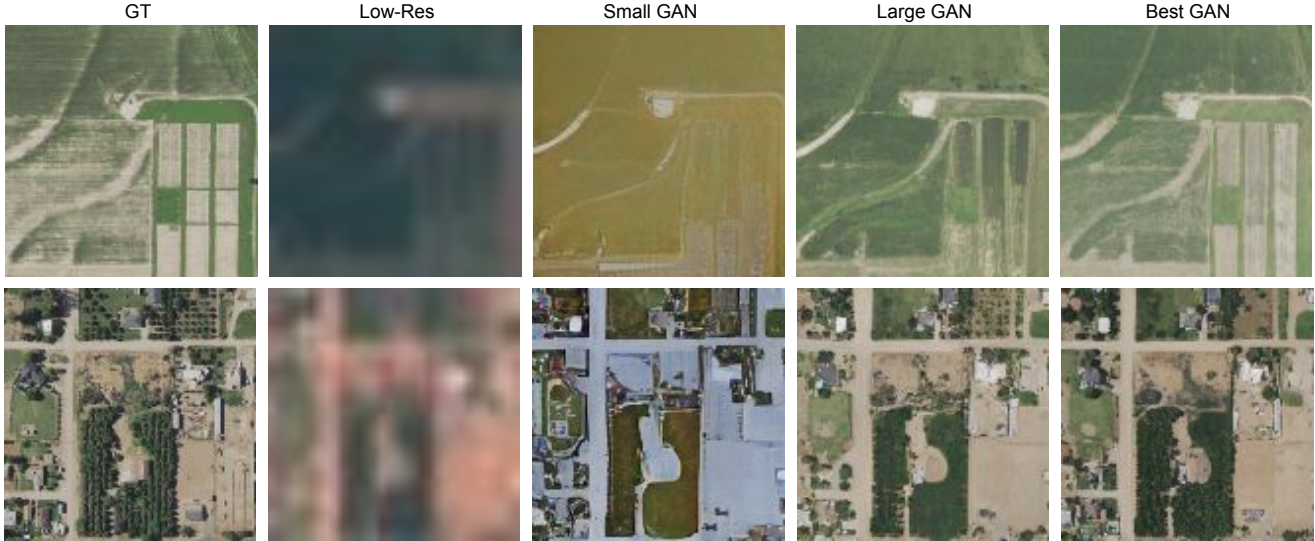


Figure 8. Examples of target images (GT), one of the corresponding low-resolution images (Low-Res), and outputs from the small, large, and best ESRGAN. We recommend zooming in and looking at the fine differences between the last two columns.

2 imagery in each of the downstream tasks, and then use them as input to a model with a Swin-Base Transformer [33] backbone pretrained on ImageNet. Second, we apply a model that inputs eight low-resolution Sentinel-2 images to the same Swin-Base Transformer [33] backbone pretrained on ImageNet. Results are shown in Table 3.

Finding 7. *Super-resolution outputs are ineffective for machine consumption.*

Via this preliminary study we find that using SUPER-RES outputs does not outperform inputting the original low-resolution images, as shown in Table 3. Interestingly, between SRCNN, HighResNet, and ESRGAN, the ESRGAN outputs led to the best average downstream performance. This suggests that optimizing L2 losses does not always imply better outputs for machine use and GANs should be considered for SUPER-RES, regardless of whether the aim is machine or human consumption.

7.2. Feature Usage

Transfer learning is a very common technique in computer vision for improving the downstream performance, though using SUPER-RES weights is largely under-explored.

We evaluate the effectiveness of this by fine-tuning a Swin-Base Transformer backbone that is (a) randomly initialized; (b) pretrained on ImageNet; (c) pretrained on SatlasPretrain [4]; and (d) pretrained on our S2-NAIP SUPER-RES dataset. And though not directly comparable, we also apply a similar model with a ResNet50 backbone pretrained using different self-supervised learning methods, including CaCo [37], SeCo [38], and SSL4EO-S12 [60]; Swin weights were not available for these methods. Results are shown in Table 4.

Input	OSM	S1	S2	S3	Big	PS	Avg
Low-Res	0.464	0.782	0.888	0.591	0.963	0.348	0.673
SRCNN	0.429	0.219	0.616	0.524	0.953	0.269	0.502
HighResNet	0.467	0.661	0.732	0.521	0.957	0.287	0.604
ESRGAN	0.486	0.723	0.706	0.524	0.954	0.299	0.615

Table 3. Results on 6 tasks (Our OpenStreetMap dataset=OSM, Satlas Tasks=Solar Farms, Wind Turbines, and Marine Infrastructure, BigEarthNet=Big, PASTIS=PS), using an ImageNet Swin Model with 8 low-resolution input images versus SUPER-RES outputs from SRCNN, HighResNet, and ESRGAN.

Finding 8. *Representations learned through super-resolution transfer to downstream tasks.*

On average, representations from SUPER-RES lead to the best downstream performance compared to those of self-supervised learning methods, CaCo [37], SeCo [38], and SSL4EO-S12 [60], and from the large-scale SatlasPretrain [4] dataset. This encourages further exploration in using SUPER-RES representations for downstream tasks.

8. Deploying Super-Resolution Globally

With all of these findings, we have deployed global SUPER-RES outputs to <https://satlas.allen.ai/> for anyone to view. We hope this can further research in AI for remote sensing as well as assist non-ML researchers with annotation tasks such as identifying the drivers of deforestation or counting green energy installations.

9. Conclusion

We explored, in depth, the metrics, datasets, and methods in the remote sensing SUPER-RES field. We propose CLIPSCORE as a new metric and utilize it to analyze three

Arch	Method	OSM	Satlas1	Satlas2	Satlas3	BigEarth	PASTIS	Avg
Res50	SeCo [38]	0.4493	0.8468	0.8962	0.6008	0.9641	0.2596	0.6695
	CaCo [37]	0.4421	0.8384	0.8985	0.5985	0.9629	0.2591	0.6666
	SSL4EO [60]	0.4529	0.8213	0.8924	0.6029	0.9637	0.2426	0.6626
Swin	Random	0.4446	0.7010	0.7391	0.5591	0.9607	0.3754	0.6299
	ImageNet	0.4642	0.7820	0.8878	0.5906	0.9631	0.3484	0.6727
	Satlas [4]	0.4718	0.8818	0.9152	0.6021	0.9641	0.3594	0.6991
	Super-Res	0.4759	0.8987	0.8958	0.5927	0.9637	0.3803	0.7012

Table 4. Transfer learning results on 6 downstream tasks (Our OpenStreetMap dataset=OSM, BigEarthNet=BigEarth, and the three Satlas tasks are Solar Farms, Wind Turbines, and Marine Infrastructure), comparing several pretraining methods to SUPER-RES weights trained on our S2-NAIP dataset.

method types, and find that GANs are very effective for this task. We introduce a new large-scale dataset, S2-NAIP, and determine the benefit of scale. We determine the effectiveness of SUPER-RES images and features for downstream tasks. Finally, these findings enable us to train a large-scale model that achieves an impressive CLIPScore.

A. Supplementary Material

The supplementary material can be accessed at [this URL](#).

References

- [1] Copernicus Sentinel Missions. <https://sentinel.esa.int/web/sentinel/home>, 2022. European Space Agency. 2
- [2] Anas M. Ali, Bilel Benjdira, Anis Koubâa, Wadii Boulila, and Walid El Shafai. Tesr: Two-stage approach for enhancement and super-resolution of remote sensing images. *Remote Sens.*, 15:2346, 2023. 2, 3
- [3] Jérémy Anger, Thibaud Ehret, Carlo de Franchis, and G. Facciolo. Fast and accurate multi-frame super-resolution of satellite images. *ISPRS Annals of the Photogrammetry, Remote Sensing and Spatial Information Sciences*, pages 57–64, 2020. 2
- [4] Favyen Bastani, Piper Wolters, Ritwik Gupta, Joe Ferdinando, and Aniruddha Kembhavi. Satlaspretrain: A large-scale dataset for remote sensing image understanding. *ICCV 2023*, 2023. 7, 8, 9
- [5] Mario Beaulieu, Samuel Foucher, Dan Haberman, and Colin Stewart. Deep image- to-image transfer applied to resolution enhancement of sentinel-2 images. *IGARSS 2018 - 2018 IEEE International Geoscience and Remote Sensing Symposium*, pages 2611–2614, 2018. 3
- [6] Goutam Bhat, Martin Danelljan, Luc Van Gool, and Radu Timofte. Deep burst super-resolution. *2021 IEEE/CVF Conference on Computer Vision and Pattern Recognition (CVPR)*, pages 9205–9214, 2021. 3
- [7] Gong Cheng, Junwei Han, and Xiaoqiang Lu. Remote Sensing Image Scene Classification: Benchmark and State of the Art. In *Proceedings of the IEEE*, pages 1865–1883, 2017. 4
- [8] Mehdi Cherti, Romain Beaumont, Ross Wightman, Mitchell Wortsman, Gabriel Ilharco, Cade Gordon, Christoph Schuhmann, Ludwig Schmidt, and Jenia Jitsev. Reproducible scaling laws for contrastive language-image learning. *2023 IEEE/CVF Conference on Computer Vision and Pattern Recognition (CVPR)*, pages 2818–2829, 2022. 4
- [9] Gordon Christie, Neil Fendley, James Wilson, and Ryan Mukherjee. Functional Map of the World. In *Proceedings of the IEEE/CVF Conference on Computer Vision and Pattern Recognition (CVPR)*, 2018. 4
- [10] Julien Cornebise, Ivan Orsolic, and Freddie Kalaitzis. Open high-resolution satellite imagery: The worldstrat dataset - with application to super-resolution. *ArXiv*, abs/2207.06418, 2022. 3, 5, 7
- [11] Michel Deudon, Alfredo Kalaitzis, Israel Goytom, Md Rifat Arefin, Zhichao Lin, Kris Sankaran, Vincent Michalski, Samira Ebrahimi Kahou, Julien Cornebise, and Yoshua Bengio. Highres-net: Recursive fusion for multi-frame super-resolution of satellite imagery. *ArXiv*, abs/2002.06460, 2020. 2, 3, 5
- [12] Chao Dong, Chen Change Loy, Kaiming He, and Xiaoou Tang. Image super-resolution using deep convolutional networks. *IEEE Transactions on Pattern Analysis and Machine Intelligence*, 38:295–307, 2014. 2, 5
- [13] Runmin Dong, Lixian Zhang, and Haohuan Fu. Rrsgan: Reference-based super-resolution for remote sensing image. *IEEE Transactions on Geoscience and Remote Sensing*, 60: 1–17, 2021. 3
- [14] Tristan Frizza, D. Dansereau, Nagita Mehr Seresht, and Michael Bewley. Semantically accurate super-resolution generative adversarial networks. *Comput. Vis. Image Underst.*, 221:103464, 2022. 2
- [15] Samir Yitzhak Gadre, Gabriel Ilharco, Alex Fang, Jonathan Hayase, Georgios Smyrnis, Thao Nguyen, Ryan Marten, Mitchell Wortsman, Dhruva Ghosh, Jieyu Zhang, Eyal Or-gad, Rahim Entezari, Giannis Daras, Sarah Pratt, Vivek Ramanujan, Yonatan Bitton, Kalyani Marathe, Stephen Mussmann, Richard Vencu, Mehdi Cherti, Ranjay Krishna, Pang Wei Koh, Olga Saukh, Alexander J. Ratner, Shuran Song, Hannaneh Hajishirzi, Ali Farhadi, Romain Beaumont, Sewoong Oh, Alexandros G. Dimakis, Jenia Jitsev, Yair Carmon, Vaishaal Shankar, and Ludwig Schmidt. Datacomp: In search of the next generation of multimodal datasets. *ArXiv*, abs/2304.14108, 2023. 4
- [16] Vivien Sainte Fare Garnot and Loic Landrieu. Panoptic segmentation of satellite image time series with convolutional temporal attention networks. *2021 IEEE/CVF International Conference on Computer Vision (ICCV)*, pages 4852–4861, 2021. 7

- [17] Jinjin Gu, Haoming Cai, Chenyu Dong, Ruofan Zhang, Yulun Zhang, Wenming Yang, and Chun Yuan. Super-resolution by predicting offsets: An ultra-efficient super-resolution network for rasterized images. In *European Conference on Computer Vision*, 2022. 3
- [18] Lintao Han, Yuchen Zhao, Hengyi Lv, Yisa Zhang, Hailong Liu, Guoling Bi, and Qing Han. Enhancing remote sensing image super-resolution with efficient hybrid conditional diffusion model. *Remote. Sens.*, 15:3452, 2023. 3
- [19] Yutong He, Dingjie Wang, Nicholas Lai, William Zhang, Chenlin Meng, M. Burke, D. Lobell, and Stefano Ermon. Spatial-temporal super-resolution of satellite imagery via conditional pixel synthesis. In *Neural Information Processing Systems*, 2021. 3
- [20] Jack Hessel, Ari Holtzman, Maxwell Forbes, Ronan Le Bras, and Yejin Choi. Clipscore: A reference-free evaluation metric for image captioning. *ArXiv*, abs/2104.08718, 2021. 2, 3, 4
- [21] Jonathan Ho. Classifier-free diffusion guidance. *ArXiv*, abs/2207.12598, 2022. 5
- [22] Jonathan Ho, Ajay Jain, and P. Abbeel. Denoising diffusion probabilistic models. *ArXiv*, abs/2006.11239, 2020. 5
- [23] Umang Jain, Alex Wilson, and Varun Gulshan. Multi-modal contrastive learning for remote sensing tasks. *ArXiv*, abs/2209.02329, 2022. 4
- [24] Minguk Kang, Jun-Yan Zhu, Richard Zhang, Jaesik Park, Eli Shechtman, Sylvain Paris, and Taesung Park. Scaling up gans for text-to-image synthesis. *2023 IEEE/CVF Conference on Computer Vision and Pattern Recognition (CVPR)*, pages 10124–10134, 2023. 2
- [25] Pawel Kowaleczko, Tomasz Tarasiewicz, Maciej Ziaja, Daniel Kostrzewa, Jakub Nalepa, Przemyslaw Rokita, and Michal Kawulok. A real-world benchmark for sentinel-2 multi-image super-resolution. *Sci Data*, 10:644, 2023. 2, 3
- [26] Nouredin Laban, Bassam Abdellatif, H. M. Ebied, Howida A. Shedeed, and Mohamed F. Tolba. Performance enhancement of satellite image classification using a convolutional neural network. In *International Conference on Advanced Intelligent System and Informatics*, 2017. 2
- [27] Xianhang Li, Zeyu Wang, and Cihang Xie. An inverse scaling law for clip training. *ArXiv*, abs/2305.07017, 2023. 4
- [28] Xianhang Li, Zeyu Wang, and Cihang Xie. Clipa-v2: Scaling clip training with 81.1% zero-shot imagenet accuracy within a \$10, 000 budget; an extra \$4, 000 unlocks 81.8% accuracy. *ArXiv*, abs/2306.15658, 2023. 4
- [29] Yunxiang Li, Meixu Chen, Wenxuan Yang, Kai Wang, Jun Ma, Alan C. Bovik, and You Zhang. Samscore: A semantic structural similarity metric for image translation evaluation. In *Arxiv*, 2023. 4
- [30] Bee Lim, Sanghyun Son, Heewon Kim, Seungjun Nah, and Kyoung Mu Lee. Enhanced deep residual networks for single image super-resolution. *2017 IEEE Conference on Computer Vision and Pattern Recognition Workshops (CVPRW)*, pages 1132–1140, 2017. 2
- [31] Chun Liu, Doudou Zeng, Hangbin Wu, Yin Wang, Shoujun Jia, and Liang Xin. Urban land cover classification of high-resolution aerial imagery using a relation-enhanced multi-scale convolutional network. *Remote. Sens.*, 12:311, 2020. 1
- [32] Jinzhe Liu, Zhiqiang Yuan, Zhaoying Pan, Yiqun Fu, Li Liu, and Bin Lu. Diffusion model with detail complement for super-resolution of remote sensing. *Remote. Sens.*, 14:4834, 2022. 2, 3
- [33] Ze Liu, Yutong Lin, Yue Cao, Han Hu, Yixuan Wei, Zheng Zhang, Stephen Lin, and Baining Guo. Swin transformer: Hierarchical vision transformer using shifted windows. *2021 IEEE/CVF International Conference on Computer Vision (ICCV)*, pages 9992–10002, 2021. 8
- [34] Tao Lu, Jiaming Wang, Yanduo Zhang, Zhongyuan Wang, and Junjun Jiang. Satellite image super-resolution via multi-scale residual deep neural network. *Remote. Sens.*, 11:1588, 2019. 2, 3
- [35] Tingyu Lu, Luhe Wan, and Lei Wang. Fine crop classification in high resolution remote sensing based on deep learning. In *Frontiers in Environmental Science*, 2022. 1
- [36] Jinming Luo, Lei Han, Xianjie Gao, Xiuping Liu, and Weiming M. Wang. Sr-feinr: Continuous remote sensing image super-resolution using feature-enhanced implicit neural representation. *Sensors (Basel, Switzerland)*, 23, 2023. 3
- [37] Utkarsh Mall, Bharath Hariharan, and Kavita Bala. Change-aware sampling and contrastive learning for satellite images. *2023 IEEE/CVF Conference on Computer Vision and Pattern Recognition (CVPR)*, pages 5261–5270, 2023. 8, 9
- [38] Oscar Mañas, Alexandre Lacoste, Xavier Giró i Nieto, David Vázquez, and Pau Rodríguez López. Seasonal contrast: Unsupervised pre-training from uncurated remote sensing data. *2021 IEEE/CVF International Conference on Computer Vision (ICCV)*, pages 9394–9403, 2021. 8, 9
- [39] Julien Michel, Juan Vinasco-Salinas, Jordi Inglada, and Olivier Hagolle. Sen2venµs, a dataset for the training of sentinel-2 super-resolution algorithms. *Data*, 7:96, 2022. 3
- [40] Volodymyr Mnih. Massachusetts buildings dataset. <https://www.kaggle.com/datasets/balraj98/massachusetts-buildings-dataset>, 2020. 2
- [41] Andrea Bordone Molini, Diego Valsesia, Giulia Fracastoro, and Enrico Magli. Deepsum: Deep neural network for super-resolution of unregistered multitemporal images. *IEEE Transactions on Geoscience and Remote Sensing*, 58: 3644–3656, 2019. 3
- [42] Marcus Mörtens, Dario Izzo, Andrej Krzic, and Daniël Cox. Super-resolution of proba-v images using convolutional neural networks. *Astrodyne*, 3:387–402, 2019. 2, 3, 5, 6, 7
- [43] Gaurav Kumar Nayak, Saksham Jain, R. Venkatesh Babu, and Anirban Chakraborty. Fusion of deep and non-deep methods for fast super-resolution of satellite images. *2020 IEEE Sixth International Conference on Multimedia Big Data (BigMM)*, pages 267–271, 2020. 2
- [44] Eduardo Pérez-Pellitero, Mehdi S. M. Sajjadi, Michael Hirsch, and Bernhard Scholkopf. Photorealistic video super resolution. *ArXiv*, abs/1807.07930, 2018. 3
- [45] Ferdinand Pineda, Victor H. Andres Ayma, and César Beltrán. A generative adversarial network approach for super-resolution of sentinel-2 satellite images. *ISPRS - International Archives of the Photogrammetry, Remote Sensing and Spatial Information Sciences*, pages 9–14, 2020. 3

- [46] Jaskaran Singh Puri and Andre Kotze. Evaluation of srgan algorithm for superresolution of satellite imagery on different sensors. *25th AGILE Conference on Geographic Information Science*, 2022. 3
- [47] Alec Radford, Jong Wook Kim, Chris Hallacy, Aditya Ramesh, Gabriel Goh, Sandhini Agarwal, Girish Sastry, Amanda Askell, Pamela Mishkin, Jack Clark, Gretchen Krueger, and Ilya Sutskever. Learning transferable visual models from natural language supervision. In *International Conference on Machine Learning*, 2021. 3, 4
- [48] Muhammed Razzak, Gonzalo Mateo-García, Luis G’omez-Chova, Yarin Gal, and Freddie Kalaitzis. Multi-spectral multi-image super-resolution of sentinel-2 with radiometric consistency losses and its effect on building delineation. *ArXiv*, abs/2111.03231, 2021. 3
- [49] Muhammed Razzak, Gonzalo Mateo-García, Luis G’omez-Chova, Yarin Gal, and Freddie Kalaitzis. Multi-spectral multi-image super-resolution of sentinel-2 with radiometric consistency losses and its effect on building delineation. *ArXiv*, abs/2111.03231, 2021. 3
- [50] Francesco Salvetti, Vittorio Mazzia, Aleem Khaliq, and Marcello Chiaberge. Multi-image super resolution of remotely sensed images using residual feature attention deep neural networks. *ArXiv*, abs/2007.03107, 2020. 2, 3
- [51] Jiaming Song, Chenlin Meng, and Stefano Ermon. Denoising diffusion implicit models. *ArXiv*, abs/2010.02502, 2020. 5
- [52] Gencer Sumbul, Marcela Charfuelan, Begüm Demir, and Volker Markl. Bigearthnet: A large-scale benchmark archive for remote sensing image understanding. *IGARSS 2019 - 2019 IEEE International Geoscience and Remote Sensing Symposium*, pages 5901–5904, 2019. 7
- [53] Quan Sun, Yuxin Fang, Ledell Yu Wu, Xinlong Wang, and Yue Cao. Eva-clip: Improved training techniques for clip at scale. *ArXiv*, abs/2303.15389, 2023. 4
- [54] Mahee Noor Tayba and P. Munoz Rivas. Enhancing the resolution of satellite imagery using a generative model. *2021 International Conference on Computational Science and Computational Intelligence (CSCI)*, pages 20–25, 2021. 2, 3
- [55] Daniel Jack Thomas, Benjamin Aubrey Robson, and Adina E. Racoviteanu. An integrated deep learning and object-based image analysis approach for mapping debris-covered glaciers. *Frontiers in Remote Sensing*, 2023. 1
- [56] Junwei Wang, Kun Gao, Zhenzhou Zhang, Chong Ni, Zibo Hu, Dayu Chen, and Qiong Wu. Multisensor remote sensing imagery super-resolution with conditional gan. *Journal of Remote Sensing*, 2021. 2, 3, 5
- [57] Peijuan Wang and Elif Sertel. Multi-frame super-resolution of remote sensing images using attention-based gan models. *Knowl. Based Syst.*, 266:110387, 2023. 2, 3
- [58] Xintao Wang, Ke Yu, Shixiang Wu, Jinjin Gu, Yihao Liu, Chao Dong, Chen Change Loy, Yu Qiao, and Xiaoou Tang. Esrgan: Enhanced super-resolution generative adversarial networks. In *ECCV Workshops*, 2018. 5
- [59] Xintao Wang, Liangbin Xie, Chao Dong, and Ying Shan. Real-esrgan: Training real-world blind super-resolution with pure synthetic data. *2021 IEEE/CVF International Conference on Computer Vision Workshops (ICCVW)*, pages 1905–1914, 2021. 2
- [60] Yi Wang, Nassim Ait Ali Braham, Zhitong Xiong, Chenying Liu, Conrad M. Albrecht, and Xiao Xiang Zhu. Ssl4eos12: A large-scale multi-modal, multi-temporal dataset for self-supervised learning in earth observation. *ArXiv*, abs/2211.07044, 2022. 8, 9
- [61] Zhou Wang, Alan Conrad Bovik, Hamid R. Sheikh, and Eero P. Simoncelli. Image quality assessment: from error visibility to structural similarity. *IEEE Transactions on Image Processing*, 13:600–612, 2004. 3
- [62] Yingfei Xiong, Shanxin Guo, Jinsong Chen, Xinpeng Deng, Luyi Sun, Xiaorou Zheng, and Wenna Xu. Improved srgan for remote sensing image superresolution across locations and sensors. *Remote. Sens.*, 12:1263, 2020. 3
- [63] Hu Xu, Saining Xie, Xiaoqing Ellen Tan, Po-Yao (Bernie) Huang, Russell Howes, Vasu Sharma, Shang-Wen Li, Gargi Ghosh, Luke Zettlemoyer, and Christoph Feichtenhofer. Demystifying clip data. *ArXiv*, abs/2309.16671, 2023. 4
- [64] Yongyang Xu, Wei Luo, Anna Hu, Zhong Xie, Xuejing Xie, and Liufeng Tao. Te-sagan: An improved generative adversarial network for remote sensing super-resolution images. *Remote. Sens.*, 14:2425, 2022. 3
- [65] Ling Yao, Tang Liu, Jun Qin, Ning Lu, and Chenghu Zhou. Tree counting with high spatial-resolution satellite imagery based on deep neural networks. *Ecological Indicators*, 125:107591, 2021. 1
- [66] Zongsheng Yue, Jianyi Wang, and Chen Change Loy. Resshift: Efficient diffusion model for image super-resolution by residual shifting. *ArXiv*, abs/2307.12348, 2023. 2
- [67] Xiaohua Zhai, Basil Mustafa, Alexander Kolesnikov, and Lucas Beyer. Sigmoid loss for language image pre-training. *ArXiv*, abs/2303.15343, 2023. 4
- [68] Richard Zhang, Phillip Isola, Alexei A. Efros, Eli Shechtman, and Oliver Wang. The unreasonable effectiveness of deep features as a perceptual metric. *2018 IEEE/CVF Conference on Computer Vision and Pattern Recognition*, pages 586–595, 2018. 3, 7
- [69] Yulun Zhang, Yapeng Tian, Yu Kong, Bineng Zhong, and Yun Raymond Fu. Residual dense network for image super-resolution. *2018 IEEE/CVF Conference on Computer Vision and Pattern Recognition*, pages 2472–2481, 2018. 2